Applied Energy 391 (2025) 125936

Contents lists available at ScienceDirect

Applied Energy

journal homepage: www.elsevier.com/locate/apenergy

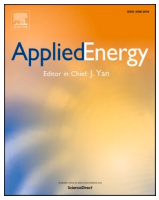

Uncovering Sodiated HC dominated thermal runaway mechanism of NFPP/HC pouch battery

Wei Li [a], Shini Lin [a], Honghao Xie [a], Yuan Qin [a], Qilong Wu [a], Jing Zeng [a,*], Peng Zhang [b,*], Jinbao Zhao [a,*]

[a] State-Province Joint Engineering Laboratory of Power Source Technology for New Energy Vehicle, State Key Laboratory of Physical Chemistry of Solid Surfaces, Engineering Research Center of Electrochemical Technology, Collaborative Innovation Center of Chemistry for Energy Materials, College of Chemistry and Chemical Engineering, Ministry of Education, Xiamen University, Xiamen 361005, China
[b] College of Energy & School of Energy Research, Xiamen University, Xiamen 361102, China

HIGHLIGHTS

- The thermal runaway mechanism of NFPP/HC pouch battery was revealed.
- Multi-level analysis methods are used to uncover the thermal runaway path.
- The serious deterioration of battery safety caused by sodium plating is emphasized.
- Ceramic coated separators are used to prevented the thermal runaway of battery.

GRAPHICAL ABSTRACT

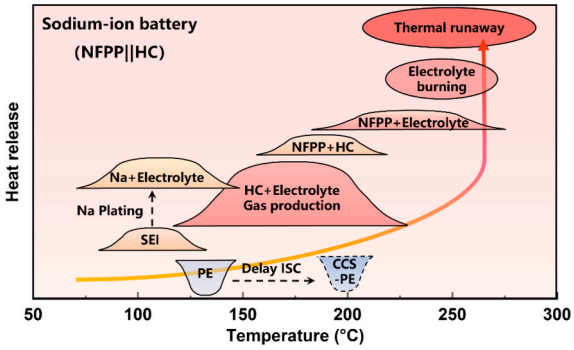

ARTICLE INFO

Keywords:
Sodium-ion batteries
Thermal runaway
Safety
Sodium plating

ABSTRACT

Sodium-ion batteries (SIBs) are considered a promising technology for large-scale energy storage systems (LSESS) because of their rich resources and outstanding electrochemical performance. However, the safety of SIBs is rarely discussed, and the thermal stability is critical to the application of the battery, especially for LSESS. In this study, the thermal runaway mechanism of $Na_3Fe_2(PO_4)(P_2O_7)$||hard carbon (NFPP/HC) pouch batteries dominated by heat generation from the sodiated anode has been uncovered. The heat generation analysis based on battery and material levels shows that the exothermic reaction between HC and the electrolyte begins to occur at 100 °C (the exothermic reaction between NFPP and the electrolyte is near 230 °C), and the reaction between the anode and electrolyte releases a large amount of heat, while NFPP materials exhibit less and milder exothermic behavior. Meanwhile, the melting temperature of the separator is extremely close to the triggering temperature of thermal runaway. Therefore, the exothermic reaction between HC and the electrolyte can cause the separator to melt, thus triggering thermal runaway of the SIBs. More seriously, when sodium plating occurs, the safety of the battery will further deteriorate. Considering the characteristic of great heat generation in the early stage of thermal runaway of SIBs, the ceramic-coated separators with higher thermal stability and higher wettability are

* Corresponding authors.
E-mail addresses: zengjing@xmu.edu.cn (J. Zeng), pengzhang@xmu.edu.cn (P. Zhang), jbzhao@xmu.edu.cn (J. Zhao).

https://doi.org/10.1016/j.apenergy.2025.125936
Received 14 January 2025; Received in revised form 26 February 2025; Accepted 10 April 2025
Available online 15 April 2025

applied to SIBs, which significantly improve battery safety. This study reveals the mechanism of thermal runaway in SIBs (NFPP/HC), which is expected to provide guidance for the research of safer SIBs.

1. Introduction

Large-scale energy storage systems (LSESS) are important technology to promote the widespread collection and efficient utilization of renewable energy [1–3]. Battery lifetime, energy storage cost, and environmental adaptability are factors that must be considered for large-scale energy storage systems applications [4,5]. Rechargeable batteries based on host-guest chemistry, which provide highly reversible electrochemical energy conversion processes and thus achieve ultra-long battery cycles, should be one of the best choices for LSESS. However, lithium-ion batteries (LIBs) might not be suitable for large-scale energy storage due to their relatively scarce lithium resource and high prices [6–8]. Instead, sodium-ion batteries (SIBs) have been recognized as ideal energy storage technologies due to their abundant resources, excellent electrochemical performance and wide operating temperature range [9,10].

In recent years, the cathode materials, anode materials, and electrolyte of SIBs have been extensively studied, and some companies have also launched their SIB energy storage products [11]. For cathode materials, polyanions, layer-structured transition metal oxides, and Prussian blue analogs have achieved commercial performance after long-term research [12–14]. Iron-based polyanionic cathode materials have received much more attention in technical applications due to their characteristics of low cost and stable structure. $Na_3Fe_2(PO_4)(P_2O_7)$ (NFPP) synthesized by Xia et al. [15] exhibited a reversible specific capacity of 110.2 mAh g^{-1} at 0.1C and the capacity retention rate of 89.7 % after 6400 cycles at 20C. For the anode, hard carbon (HC) has an absolute advantage due to its large reversible sodium storage capacity and low working potential. HC has also been extensively studied in terms of synthesis methods [16–18], sodium storage mechanisms [19,20], and SEI formation [21,22]. Therefore, SIBs composed of polyanion cathode and HC anode have become the most popular technologies in the research and industrial application of energy storage systems [23,24]. The multi-faceted performance of three types of energy storage batteries has also been compared, and NFPP/HC batteries have advantages in all aspects except energy density, which once again proves the application prospects of NFPP/HC (Scheme 1).

Although the electrochemical performance of SIBs materials has been widely studied, systematic results and discussion on the thermal stability and heat generation behavior at the material and battery levels are still lacking. Safety and thermal runaway research are essential aspects of new energy storage technologies, especially for large-scale energy storage systems applications [25–27]. As far as we know, except for a report from Hu's team evaluating the thermal runaway of SIBs with layered cathode, almost no work has focused on the safety characteristics of SIBs. [28] The flammability of the electrolyte, the structural stability of the cathode material, the thermal stability of the sodiated anode, the crosstalk effect inside the battery, and the internal gas production will be safety hazards for the application of SIBs [29–32]. Therefore, during the application of SIBs, it is urgent to conduct comprehensive safety testing and gain insight into their sources of heat release in order to clarify the direction of subsequent research.

Herein, we systematically explored the detailed thermal failure of 5 Ah SIBs with NFPP cathode and HC anode. The batteries have shown high stability in mechanical abuse, electrical abuse, and thermal abuse tests. Benefiting from accelerated rate calorimetry (ARC) and differential scanning calorimetry (DSC), the thermal runaway path and internal materials decomposition mechanism of SIBs have been discovered. The thermal analysis experiment about the battery and its internal materials combination found that the heat generated during thermal runaway mainly comes from the reaction between the sodiated anode and electrolyte, while the reaction between the cathode and electrolyte is very weak (only 1/3 of the anode side). And the exothermic reaction on the HC begins to occur at 100 °C, while the exothermic reaction on the NFPP starts at 234 °C. X-ray diffraction (XRD) and scanning electron microscopy (SEM) results certify that the cathode material still maintains structural stability at 400 °C without electrolyte. For the HC, the titration gas chromatography (TGC) proved that the heat release on the anode side mainly comes from the exothermic reaction between the electrolyte and sodium in HC materials. Subsequently, SIBs with sodium plating were used for thermal failure analysis, and it was found that sodium plating on the anode would significantly reduce the self-generated heat temperature and thermal runaway triggering temperature of the battery, while greatly improving the temperature rise rate during thermal runaway. Compared to LIBs, SIBs exhibit more significant self-generated heat in the early stages. However, the thermal runaway is more alleviated due to the ultra-high thermal stability of the cathode and the lower energy density of SIBs. For the low thermal runaway trigger temperature of SIBs, ceramic-coated separators (PE-CCS) with higher thermal stability are used to replace polyethylene separators (PE), which significantly improves battery safety. Meanwhile, PE-CCS also effectively suppresses sodium plating caused by incomplete wetting. Our work reveals sodiated HC dominated thermal runaway mechanism of SIBs, which will shed new light on the way forward for developing SIBs with high safety performance.

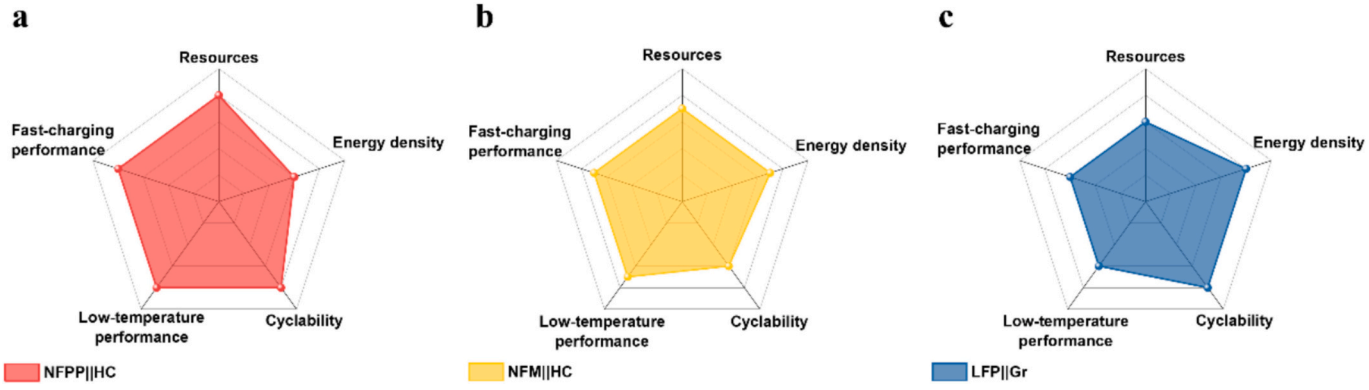

Scheme 1. Performance comparison of three types energy storage batteries of (a) HC||NFPP, (b) HC||$NaNi_{1/3}Fe_{1/3}Mn_{1/3}O_2$ (HC||NFM) and (c) Graphite||$LiFePO_4$ (Gr||LFP).

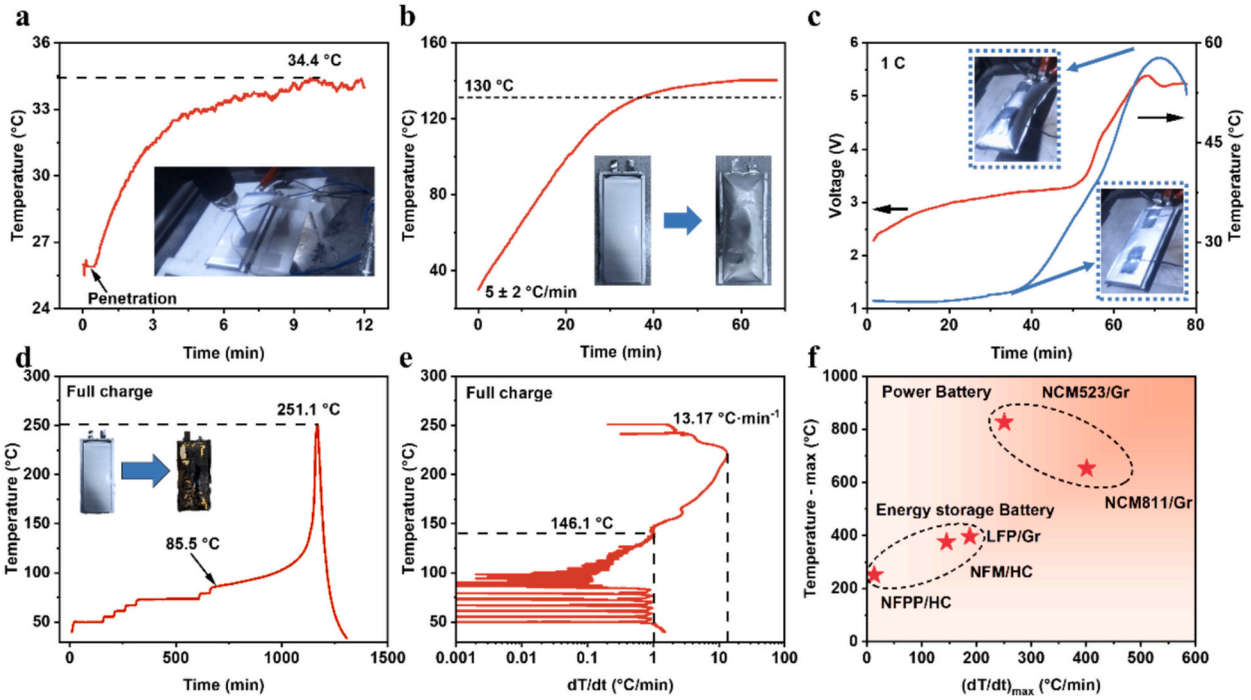

Fig. 1. Temperature profiles of the SIBs pouch battery under (a) nail penetration test and (b) thermal abuse test. (c) Temperature and voltage profiles of the SIBs under overcharge test. (d, e) The heat-wait-search curves of fully charged 5 Ah SIBs. (f) Comparison of thermal runaway characteristic temperatures. (Comparing batteries including NCM523/Gr [33], NCM811/Gr [34], LFP/Gr (this work), NFM/HC (our unpublished work) and NFPP/HC (this work)).

2. Results and discussion

Excellent electrochemical performance is a prerequisite for battery safety research. The 5 Ah NFPP/HC pouch battery with 1 M $NaPF_6$ in EC/PC/DEC displayed a stable capacity retention rate of 95.9 % after 200 cycles at 1C, the coulombic efficiency remained consistently above 99.9 % (Fig. S1 (a, b)). In addition, the battery exhibits excellent rate performance (Fig. S1 (c)). Its mass energy density reaches 100.0 Wh/Kg (Table S2). The outstanding cycling performance indicates that the electrochemical performance of the battery is acceptable, and the safety analysis based on the battery is reasonable and convincing. For large-scale energy storage, evaluating the thermal runaway characteristics under abusive conditions is crucial for developing safe batteries. Here, the fully charged SIBs pouch batteries are used for abuse testing according to international standards, including nail penetration test, overcharging test, and hot-box test. In the nail penetration test, the temperature of the battery slowly rises to 34.4 °C without any smoke or fire within 12 min (Fig. 1. (a)). In the hot-box test, the battery was heated at a rate of 5 ± 2 °C min^{-1}, and was maintained for 30 mins when the temperature reached 130 °C. During the testing process, the battery only experiences gas production without any smoke or fire, and the temperature of the battery does not experience any sudden changes (Fig. 1. (b)). In the overcharge test, the battery was charged to 1.5 times the upper limit voltage (3.9 V) by a current of 1C. During this process, the temperature of the battery reached a maximum of 57.7 °C, and then the temperature drops. Besides, the voltage of the battery fluctuated around 5.2 V (Fig. 1. (c)). After the battery was disassembled, there is severe sodium plating on the surface of HC and separator, and sodium dendrites penetrating the separator can be seen on the surface of NFPP (Fig. S2 (a-d)). The abuse test results following international standards indicate that fully charged batteries have sufficient reliability in the early stages of use, but there are also some phenomena such as temperature rise and gas generation, which require further exploration of safety evolution under adiabatic conditions and in the later stages of use.

The thermal runaway characteristics of SIBs pouch batteries were studied using the HWS (Heat-Wait-Search) mode of ARC, and adiabatic conditions were simulated by maintaining the experimental chamber temperature consistent with the battery temperature (the testing method is shown in the Fig. S3). During the ARC testing process, a series of key parameters were recorded, including the starting temperature of self-generation heat (T_1), the triggering temperature of thermal runaway (T_2, defined as dT dt^{-1} = 1 °C min^{-1}), the maximum temperature of thermal runaway (T_3), and the maximum rate of temperature rise during thermal runaway ((dT dt^{-1})$_{max}$). Self-generation heat is believed to be caused by the decomposition heat of SEI and the exothermic reaction between the metal plating on the anode surface and the electrolyte. T_2 is the tipping point that separates the mild temperature increase from the sharp temperature increase [25], and the main influencing factors include the internal crosstalk reaction of batteries, separator contraction, etc.

In safety analysis, thermal runaway characteristics of NFPP/HC SIBs were compared with $LiFePO_4$/Graphite (LFP/Gr) LIBs, because the LFP/Gr LIBs being the main technological means of electrochemical energy storage at present. The selected LFP/Gr have excellent electrochemical performance, and their capacity and size are close to those of NFPP/HC (Fig. S4 (a, b), Table S3). The T_1 of fully charged SIBs is located at 85.5 °C, indicating that the exothermic reactions of SIBs begin at 85.5 °C (SEI decomposition), which is lower than the 95.8 °C of LFP/Gr (Fig. S4 (c, d)). The following exothermic reactions drive the battery to continuously heat up until thermal runaway. T_2 of NFPP/HC and LFP/Gr are located at 146.1 °C and 182.3 °C respectively, which means that massive exothermic reactions occur inside the battery. The SEI decomposition heat release of SIBs will be higher than that of LIBs, because of the high activity of sodium metal (Fig. 5 (a)), which will result in a more drastic exothermic reaction in the early stages of thermal runaway, so that the T_1 and T_2 decrease. In addition, the characteristic temperatures of T_1 and T_2 are closer, under extreme abuse conditions, it is highly likely to break through the two characteristic temperatures in a short period of time. Therefore, it is particularly important to clamp the heat generation of the SIBs in the early stage of thermal runaway.

After T_2, the battery temperature exponentially increases until it explodes. The maximum temperature of thermal runaway (T_3) is

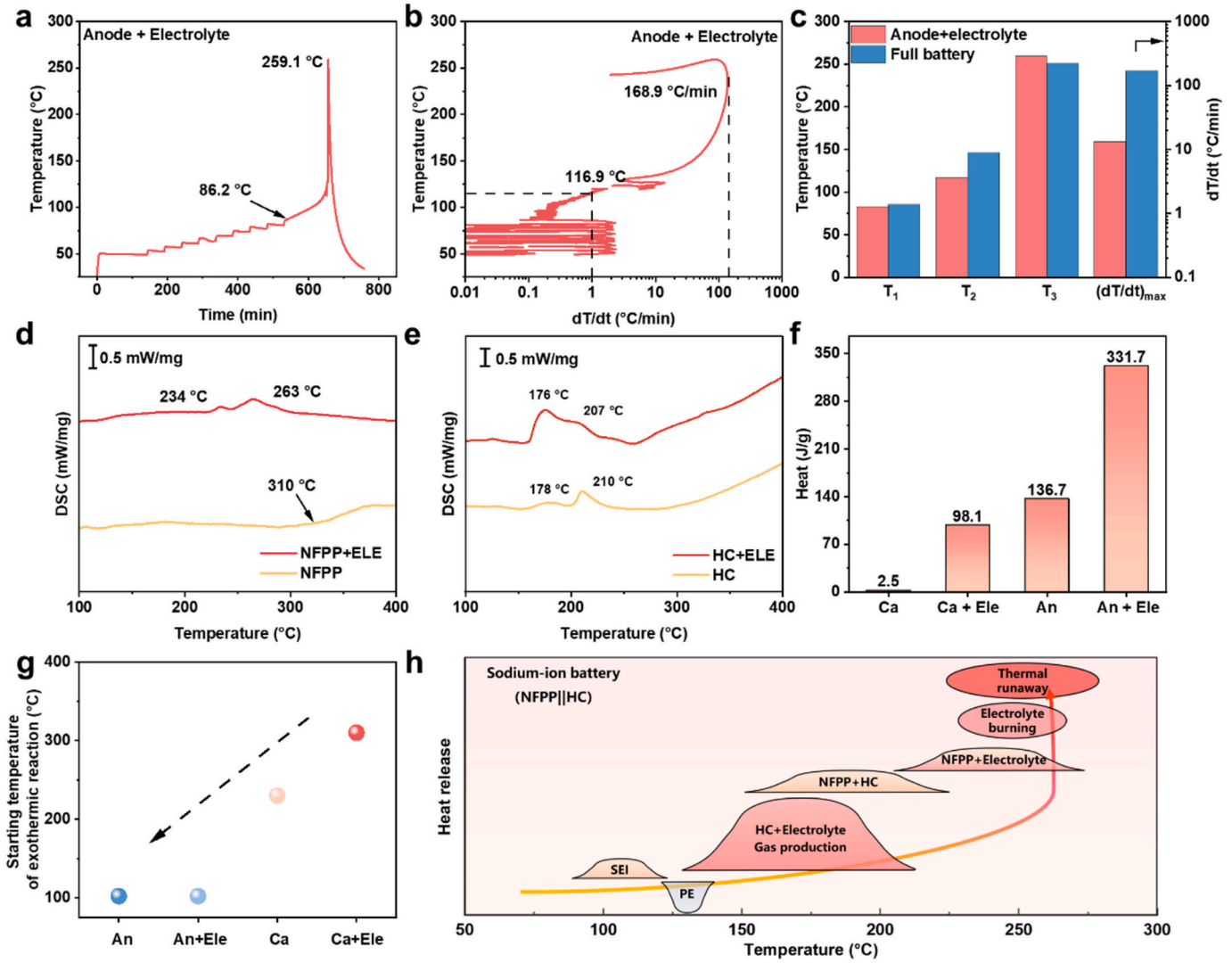

Fig. 2. (a, b) ARC test result of partial battery (anode and electrolyte). (c) Comparison of characteristic temperatures between partial battery (anode and electrolyte) and full battery. (d) DSC test result of fully charged NFPP and its mixtures with electrolyte. (e) DSC test result of fully charged HC anode and its mixtures with electrolyte. (f) Heat generation of the NFPP and HC of full charged SIBs. g) Exothermic reaction starting temperature of the NFPP and HC of full charged SIBs. (h) The heat release diagram of NFPP/HC (In this figure, An, Ca and Ele represent the HC, NFPP, and electrolyte, respectively).

251.1 °C, and the $(dT\ dt^{-1})_{max} = 13.17\ °C\ min^{-1}$ (Fig. 1 (d, e)). In sharp contrast, the T_3 and the $(dT\ dt^{-1})_{max}$ of LFP/Gr reached 396.1 °C and 187.8 °C min^{-1} respectively (Fig. S4 (c, d)). In addition, the $(dT\ dt^{-1})_{max}$ is positively correlated with the energy density of the battery [25]. As the energy density of SIBs is smaller than that of LIBs, both $(dT\ dt^{-1})_{max}$ and T_3 are significantly reduced (Fig. 1 (f)), the hazard level of SIBs is significantly reduced. For the discharged battery, it independently underwent exothermic reactions at three temperature points: 110.1 °C, 163.5 °C, and 201.3 °C in HWS mode (Fig. S5 (a, b)). After being heated to the upper limit of the test temperature, there is no thermal runaway detected in the battery, demonstrating extremely high safety. Overall, the hazard of thermal runaway of SIBs is significantly reduced compared to LIBs, but the heat generated in the early stage of thermal runaway is relatively large and develops rapidly. Therefore, it is necessary to find strategies and elements to restrain its development. Moreover, the exothermic reactions in the SIBs that lead to thermal runaway still need to be further studied at the materials level of the cathode, anode and electrolyte.

In order to decouple the exothermic reactions inside the fully charged SIBs and identify the major heat contributions to the thermal runaway process, partial batteries were assembled to explore the detailed reactions within the materials. Both cathode and anode materials were obtained from disassembled fully charged SIBs. Among the ARC tests of partial batteries, only the anode-electrolyte partial battery begins to generate heat at a lower temperature, and experiences continuous and significant heat generation, resulting in a sharp increase of battery temperature (Fig. 2 (a, b), Fig. S6). This partial battery begins to generate heat at 86.2 °C, which is close to that of the full battery. Subsequently, we noticed that the anode-electrolyte partial battery experiences sharp increase of battery temperature, with T_2 being 116.9 °C, which is 30 °C lower than that of the full battery. Moreover, the $(dT\ dt^{-1})_{max}$ of the anode-electrolyte partial battery reaches 168.9 °C min^{-1}, which is more than 10 times higher than that of the full battery (Fig. 2 (c)). The comparison of ARC test results between full batteries and partial batteries indicates that the exothermic reaction of the anode-electrolyte is the main heat source for self-generated heat and thermal runaway of the battery, and the NFPP has high thermal stability. Moreover, the NFPP shares the heat generated from the anode and electrolyte, reducing the temperature rise rate during battery thermal runaway.

DSC was also used to accurately quantify the thermal contributions of electrode materials with and without electrolyte. The cathode and

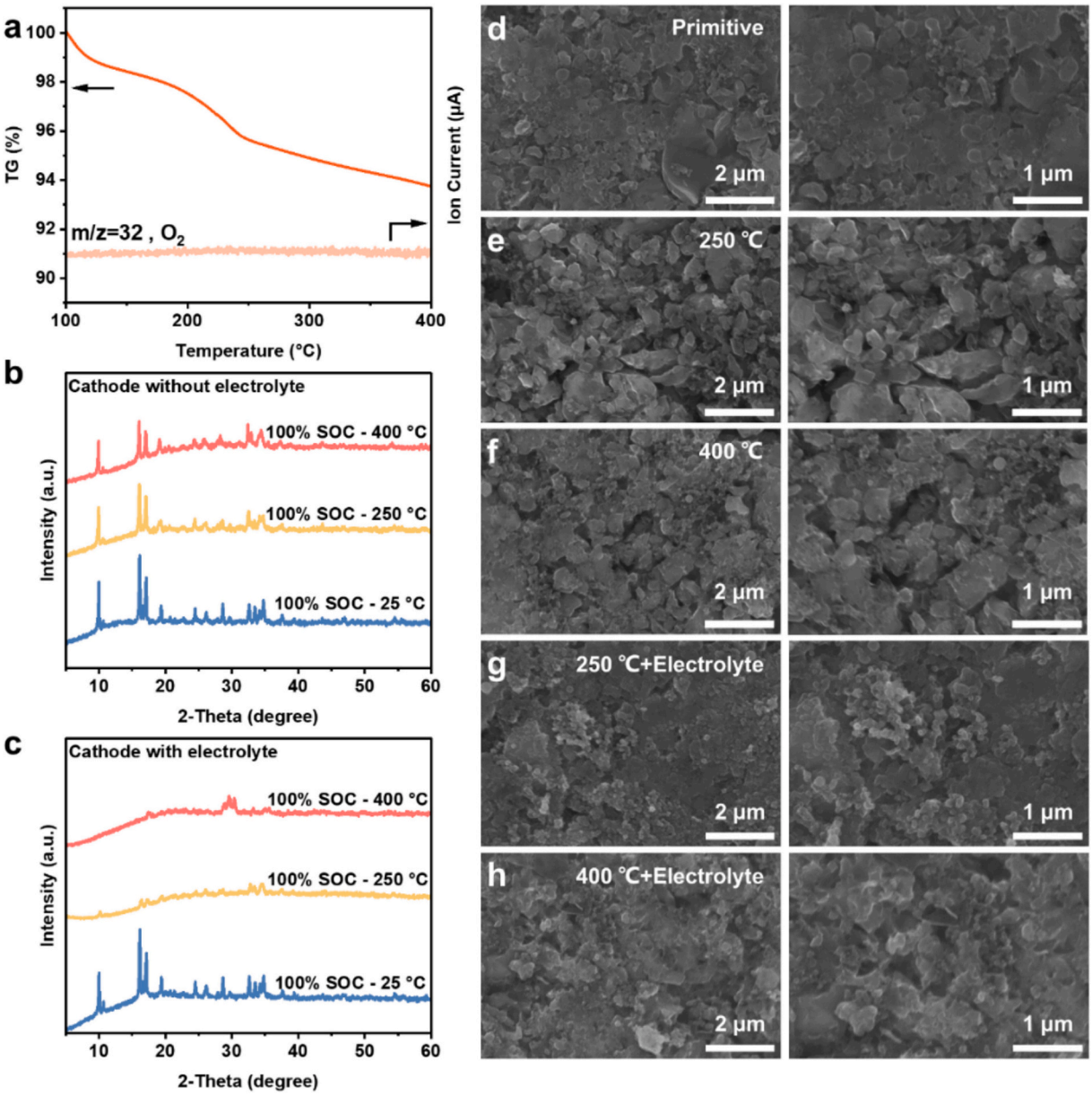

Fig. 3. (a) Test results of TG-MS: the oxygen release signal curve and weight loss curve of fully charged NFPP cathode. XRD patterns for (b) fully charged NFPP cathode (c) fully charged NFPP cathode mixtures with electrolyte. SEM images of fully charged NFPP processed under different conditions: (d) primitive, (e) 250 °C without electrolyte, (f) 400 °C without electrolyte, (g) 250 °C with electrolyte, (h) 400 °C with electrolyte.

anode materials in DSC test were also disassembled from fully charged SIBs, and the detailed test settings are shown in Table S4. In the DSC testing, the desodiated NFPP showed extremely high thermal stability, with an exothermic peak only appearing at 310 °C. In the NFPP and electrolyte system, two mild exothermic peaks were observed at 234 °C and 263 °C (Fig. 2 (d)). The exothermic peak may be attributed to the reaction between the desodiated NFPP and the electrolyte, because the electrolyte itself does not undergo an exothermic reaction before 300 °C (Fig. S7). In summary, the NFPP-related exothermic reaction occurs a temperature higher than 230 °C, and the exothermic peak is relatively gentle. Conversely, both sodiated HC and sodiated HC-electrolyte mixture showed significant exothermic peaks around 176 °C and 207 °C, and the mixture had more heat release (Fig. 2 (e)). TGC testing confirms that these two exothermic peaks were attributed to the reaction between the electrolyte and sodium in HC (Fig. S9). By comparing the heat release and the starting temperature of the exothermic reaction between the NFPP and the electrolyte, and between the HC and the electrolyte, it is found that the heat production of the HC-electrolyte system was three times that of the NFPP-electrolyte system, and the exothermic reaction was advanced by 130 °C. It is proved once again that the exothermic reaction of sodiated HC is the main heat source for the initiation of self-generation heat and thermal runaway of SIBs (Fig. 2 (f, g)). Moreover, it has been demonstrated in some studies that the reducing gas generated at the anode-electrolyte interface accelerates the thermal runaway of the battery. Consequently, we conducted further analysis on the gas composition [35]. HC and electrolyte are sealed in the aluminum-plastic film and heated at 100 °C for 1 h; a large amount of gas is generated (Fig. S10 (a)). Through GC analysis, it was found that the main components of the gas are flammable gases such as H_2 and unsaturated hydrocarbons (Fig. S10 (b)). The TG-MS test results of the HC and electrolyte mixture also confirmed the occurrence of gas production (Fig. S11). And the temperature of gas generation of the mixture and DSC exothermic peak basically coincides. The generation of combustible gases between sodiated HC and the electrolyte poses great

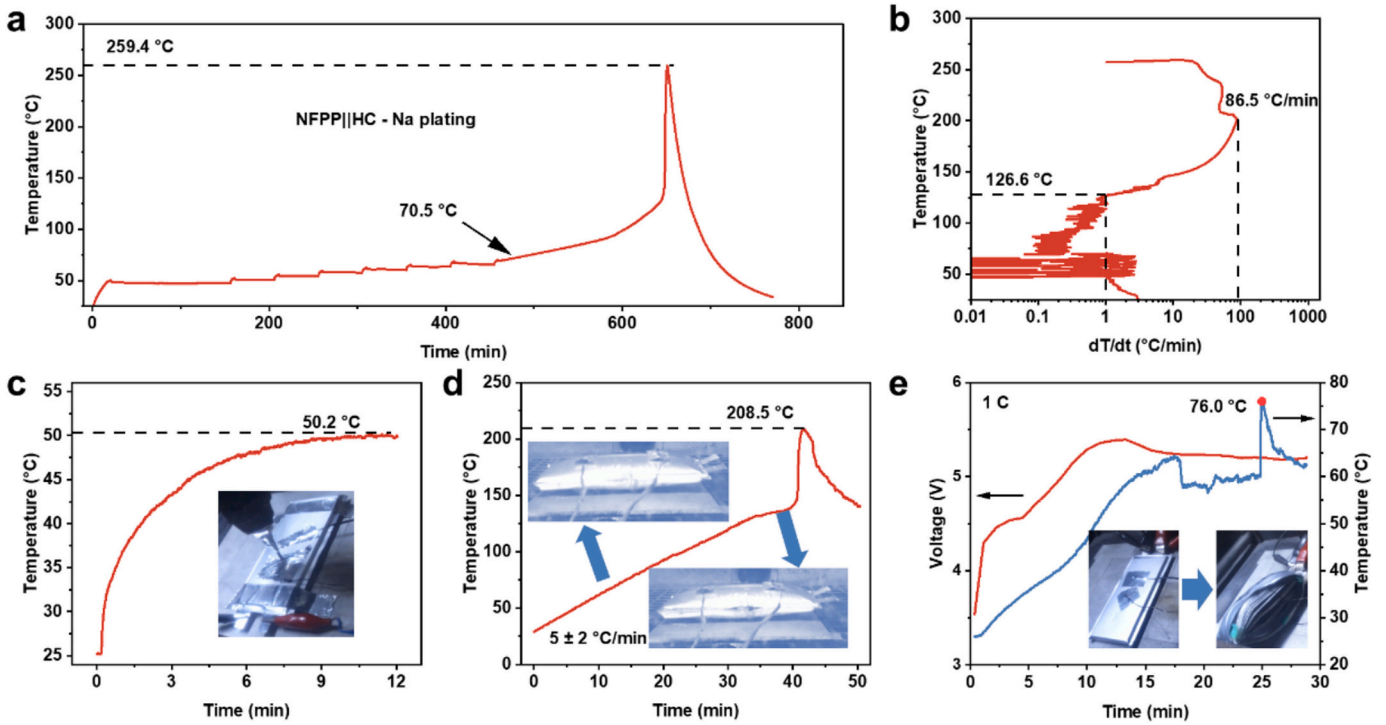

Fig. 4. (a, b) The heat-wait-search curves of fully charged 5 Ah SIBs with anode sodium plating. Abuse testing of the SIBs pouch battery with anode sodium plating: (c) Nail penetration test; (d) Thermal abuse test; (e) Overcharge test.

risks to the safety of batteries and will further exacerbate the severity of thermal runaway.

The post-mortem analysis of reaction products under high temperatures was performed to unveil the thermal failure mechanisms of NFPP and NFPP with electrolyte. TG-MS was used to study the decomposition of desodiated NFPP under high temperature conditions. The weight loss rate of NFPP within the testing range of 100–400 °C is only 6 %. It is speculated that this weight loss may be caused by the decomposition of trace amounts of residual electrolyte and conductive carbon on the surface. Besides, there was no release of oxygen during the testing process (Fig. 3 (a)). These test results preliminarily demonstrate the structural stability of desodiated NFPP at high temperatures. According to the DSC test results of the cathode materials and electrolyte, the reaction products of the NFPP (with and without electrolyte) after heating at 25 °C, 250 °C and 400 °C were investigated in detail. As shown in XRD and SEM results (Fig. 3 (b-h)), in the absence of the electrolyte, there is no significant deterioration of the structure and surface morphology of NFPP materials when heated to 250 °C and 400 °C. However, in the mixture of the cathode and the electrolyte, the crystal structure of the NFPP has already been destroyed at 250 °C, and the morphology of the cathode materials has also changed. When the temperature reaches 400 °C, the material is further damaged, and the boundary of the cathode particles becomes irregular. These results further prove that the heat generation at the the cathode-electrolyte interface is caused by the erosion of the electrolyte on the cathode material (The sample preparation and testing methods are shown in Fig. S8). In summary, desodiated NFPP materials maintain excellent stability, and the heat release is very weak even when mixed with the electrolyte.

The lithium plating of LIBs not only deteriorates battery performance, but also poses a risk to the reliability of the battery, and even triggers thermal runaway [33,36]. Sodium metal has higher surface area and high activity, and the safety hazards brought by sodium plating cannot be ignored. In the thermal analysis of sodium plating, SIBs were cycled at 3C for 100 cycles to trigger sodium plating of HC. The HC potential of the pouch battery with reference electrode (RE) and optical image of HC after cycling indicate sodium plating on the anode of the SIBs when cycling at 3C for 100 cycles (Fig. S12 (a - d). Subsequently, the full-charge battery after fast charge was tested by ARC (Fig. 4 (a, c)). The experimental results indicate that the sodium plating significantly lowered the T_1 (decreased from 85.5 °C to 70.5 °C) and T_2 (decreased from 146.1 °C to 126.6 °C). This is because the sodium plating has a high specific surface area and high activity, and it induces the continuous formation of SEI, thus leading to lower T_1. At the same time, the $(dT/dt)_{max}$ increased from 13.17 °C min^{-1} to 86.5 °C min^{-1}. Sodium plating increases the heat generation at the interface of the anode-electrolyte, thermal runaway of the battery occurs more easily and more violently due to the accumulation of heat.

Subsequently, fast-charged SIBs were used for abuse testing as shown in Fig. 4 (c - d) (test conditions are the same as Fig. 1 (a - c)). In the acupuncture test, the battery was slowly heated to 50.2 °C after being punctured, and there is no smoke and fire phenomenon. However, compared with conventional batteries, the temperature is increased by 15.8 °C. In the heat abuse test, the SIBs after fast charging showed a rapid temperature increase at around 139 °C, with the highest temperature reaching 208.5 °C. However, the battery only experienced gas expansion and shell breakage, without smoke and fire. In the overcharging test, the battery voltage quickly reached 5.38 V, but due to internal side reactions, the voltage slightly decreased and eventually stabilized around 5.2 V. During overcharging, the battery temperature slowly rose to 64.1 °C, followed by a sudden increase to 76.0 °C. However, the battery only experience expansion and rupture of the aluminum-plastic film, without any occurrence of fire. Thus, the abuse testing further demonstrates the critical role of sodium plating during thermal runaway of the NFPP/HC battery. In addition, some studies have shown that sodium plating will lead to the generation of reducing gases such as hydrogen, which will also deteriorate the safety of SIBs [37,38]. To sum up, sodium plating will significantly reduce the reliability of the battery and increase the severity of thermal runaway.

After the safety analysis of SIBs in their early life and sodium plating state, we found that the thermal runaway triggering temperature of SIBs was at a low temperature (120–150 °C). In addition, the heat source of the process was mainly the SEI decomposition heat production on the

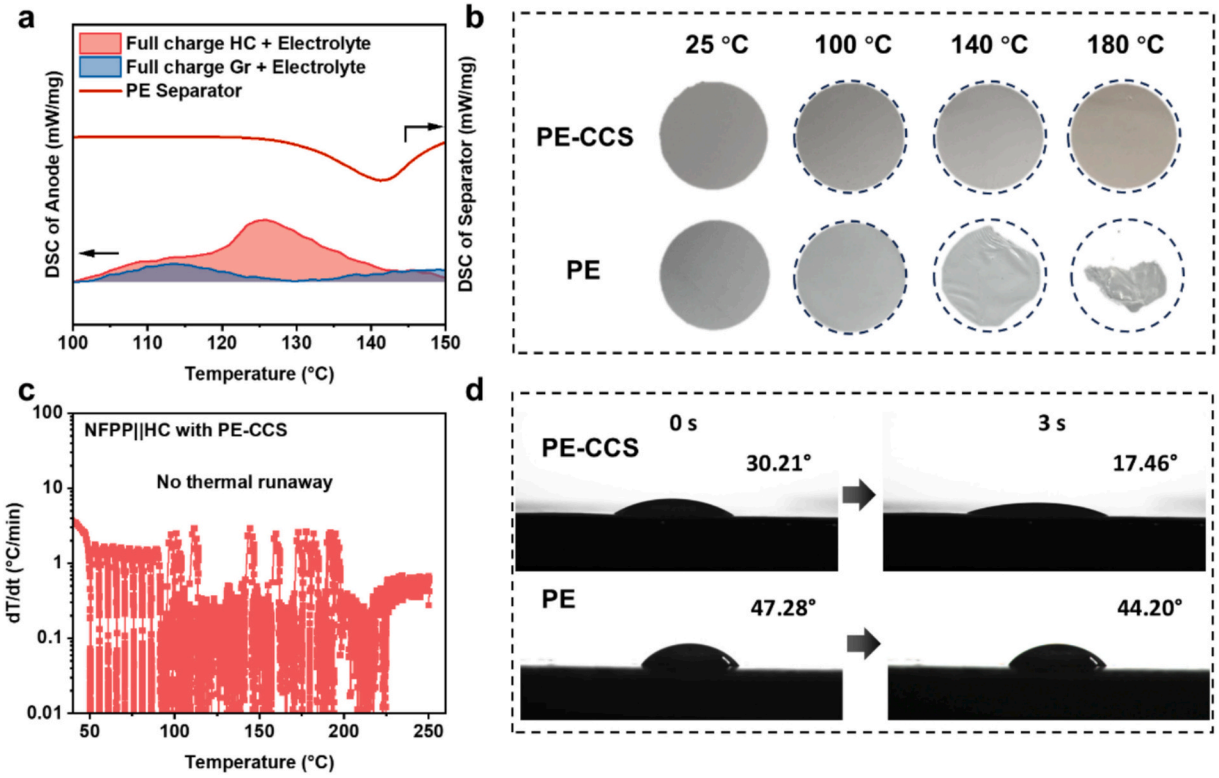

Fig. 5. (a) Exothermic behavior of the HC and Gr of full charged SIBs and LIBs, and endothermic behavior of the PE Separator. (b) Optical image of the PE, PE-CCS separators after the thermal shrinkage test at various temperatures for 30 mins. (c) The heat-wait-search curves of fully charged 5 Ah SIBs with PE-CCS. (d) Contact angles of PE and PE-CCS.

HC (Fig. 5 (a)). Coincidentally, the temperature range was consistent with the melting temperature of the PE separator (Fig. 5 (b)). Therefore, we conclude the key mechanism of thermal runaway triggering: the decomposition reaction of SEI generates heat, raises the battery temperature to the separator melting temperature, resulting in large-scale internal short circuit of the battery, and thermal runaway is triggered (Fig. 5 (c)). For this phenomenon, the PE-CCS separator with higher thermal stability is used to replace the ordinary PE separator. The surface of the PE-CCS separator is coated with a layer of excellent heat-resistance Al_2O_3 inorganic ceramic particles, which greatly improves the shrinkage resistance of the separator (Fig. S13). In heat-shrinkage experiments of separator, PE-CCS separator showed excellent thermal stability, maintaining dimensional stability at 180 °C, while PE began to shrink near 140 °C (Fig. 5 (d)). Finally, the SIBs with PE-CCS separator demonstrated high safety in ARC testing without thermal runaway (Fig. 5 (e)). Meanwhile, the high wettability of PE-CCS towards electrolytes has been demonstrated through contact angle testing. Typically, batteries that are not fully wetted may experience localized sodium plating due to residual gases and higher internal resistance [39–41]. Therefore, PE-CCS also effectively suppresses sodium plating caused by incomplete wetting. Herein, we present the key points of SIBs thermal runaway and significantly improve battery safety through a simple PE-CCS separator strategy.

3. Conclusion

In this work, the thermal runaway mechanism of 5 Ah SIBs (NFPP/HC) has been successfully revealed. The battery exhibited excellent thermal stability and did not exhibit thermal runaway behavior during abuse testing in the early stages of use. Through thermal analysis of SIBs at the battery and material levels, we found that the heat generated during the thermal runaway process mainly came from the exothermic reaction between the sodiated HC and the electrolyte, which occurs around 100–150 °C. The heat provided by the exothermic reaction also caused the separator to melt, triggering internal short circuit and thermal runaway. However, the desodiated NFPP exhibits excellent thermal stability, and its reaction heat release with the electrolyte is very weak (only 1/3 of the anode side). Therefore, sodiated HC was a key factor to induce heat production and to trigger thermal runaway. More seriously, after sodium plating on HC, the T_1 and T_2 of the battery were significantly reduced, while the $(dT/dt)_{max}$ was greatly increased. In addition, SIBs with sodium plating also exhibited poor thermal stability during abuse testing. Finally, we significantly improved the safety of batteries with our simple ceramic separator technology. These findings uncovered the heat sources and triggering factors of SIBs' thermal runaway, and will provide valuable recommendations for the design and development of safer SIBs and materials.

CRediT authorship contribution statement

Wei Li: Writing – original draft, Investigation, Formal analysis, Data curation, Conceptualization. **Shini Lin:** Investigation, Formal analysis, Conceptualization. **Honghao Xie:** Investigation, Data curation. **Yuan Qin:** Investigation. **Qilong Wu:** Data curation. **Jing Zeng:** Writing – review & editing, Funding acquisition. **Peng Zhang:** Writing – review & editing, Funding acquisition. **Jinbao Zhao:** Writing – review & editing, Funding acquisition, Conceptualization.

Declaration of competing interest

The authors declare that they have no known competing financial interests or personal relationships that could have appeared to influence the work reported in this paper.

Acknowledgements

We gratefully acknowledge the financial supported by National Key Research and Development Program of China (2021YFB2400300), Yunnan Major Scientific and Technological Projects (202202AG050003), and Natural Science Foundation project of Xiamen city (No. 3502Z202471026).

Appendix A. Supplementary data

Supplementary data to this article can be found online at https://doi.org/10.1016/j.apenergy.2025.125936.

Data availability

Data will be made available on request.

References

[1] Guo Y-J, Jin R-X, Fan M, Wang W-P, Xin S, Wan L-J, et al. Sodium layered oxide cathodes: properties, practicality and prospects. Chem Soc Rev 2024;53:7828–74. https://doi.org/10.1039/D4CS00415A.
[2] Hu X, Li H, Wang Z, Liu M, Lu Y, Zhang Y, et al. High Entropy Helps Na4Fe3(PO4)2P2O7 Improve Its Sodium Storage Performance. Adv Funct Mater 2025:2412730. https://doi.org/10.1002/adfm.202412730.
[3] Liu T, Zhang Y, Jiang Z, Zeng X, Ji J, Li Z, et al. Exploring competitive features of stationary sodium ion batteries for electrochemical energy storage. Energy Environ Sci 2019;12:1512–33. https://doi.org/10.1039/C8EE03727B.
[4] Wang Y, Lan H, Dong S, Zhu Q, Cheng L, Wang H, et al. A High-Power Rechargeable Sodium-Ion Full Battery Operating at −40 °C. Adv Funct Mater 2025:2315498. https://doi.org/10.1002/adfm.202315498.
[5] Niu Y-B, Guo Y-J, Yin Y-X, Zhang S-Y, Wang T, Wang P, et al. High-efficiency cathode sodium compensation for sodium-ion batteries. Adv Mater 2020;32:2001419. https://doi.org/10.1002/adma.202001419.
[6] Hijazi H, Ye Z, Zhang L, Deshmukh J, Johnson MB, Dahn JR, et al. Impact of sodium metal plating on cycling performance of layered oxide/hard carbon sodium-ion pouch cells with different voltage cut-offs. J Electrochem Soc 2023;170:070512. https://doi.org/10.1149/1945-7111/ace4fa.
[7] Li Y, Vasileiadis A, Zhou Q, Lu Y, Meng Q, Li Y, et al. Origin of fast charging in hard carbon anodes. Nat Energy 2024;9:134–42. https://doi.org/10.1038/s41560-023-01414-5.
[8] Usiskin R, Lu Y, Popovic J, Law M, Balaya P, Hu Y-S, et al. Fundamentals, status and promise of sodium-based batteries. Nat Rev Mater 2021;6:1020–35. https://doi.org/10.1038/s41578-021-00324-w.
[9] Gao Y, Zhang H, Peng J, Li L, Xiao Y, Li L, et al. A 30-year overview of sodium-ion batteries. Carbon Energy 2024;6:e464. https://doi.org/10.1002/cey2.464.
[10] Glushenkov AM. Recent commentaries on the expected performance, advantages and applications of sodium-ion batteries. Energy Mater 2023;3. https://doi.org/10.20517/energymater.2022.70. N/A-N/A.
[11] Yang H, Zhang Q, Chen M, Yang Y, Zhao J. Unveiling the origin of air stability in Polyanion and layered-oxide cathode materials for sodium-ion batteries and their practical application considerations. Adv Funct Mater 2024;34:2308257. https://doi.org/10.1002/adfm.202308257.
[12] Ding F, Zhao C, Zhou D, Meng Q, Xiao D, Zhang Q, et al. A novel Ni-rich O3-Na[Ni0.60Fe0.25Mn0.15]O2 cathode for Na-ion batteries. Energy Storage Mater 2020;30:420–30. https://doi.org/10.1016/j.ensm.2020.05.013.
[13] Gao S, Zhu Z, Fang H, Feng K, Zhong J, Hou M, et al. Regulation of coordination chemistry for Ultrastable layered oxide cathode materials of sodium-ion batteries. Adv Mater 2024;36:2311523. https://doi.org/10.1002/adma.202311523.
[14] Li L, Hu Z, Lu Y, Wang C, Zhang Q, Zhao S, et al. A low-strain potassium-rich Prussian blue analogue cathode for high power potassium-ion batteries. Angew Chem Int Ed 2021;60:13050–6. https://doi.org/10.1002/anie.202103475.
[15] Cao Y, Yang C, Liu Y, Xia X, Zhao D, Cao Y, et al. A new Polyanion Na3Fe2(PO4)P2O7 cathode with high electrochemical performance for sodium-ion batteries. ACS Energy Lett 2020;5:3788–96. https://doi.org/10.1021/acsenergylett.0c01902.
[16] Li Y, Lu Y, Meng Q, Jensen ACS, Zhang Q, Zhang Q, et al. Regulating pore structure of hierarchical porous waste Cork-derived hard carbon anode for enhanced Na storage performance. Adv Energy Mater 2019;9:1902852. https://doi.org/10.1002/aenm.201902852.
[17] Liu J, You Y, Huang L, Zheng Q, Sun Z, Fang K, et al. Precisely tunable instantaneous carbon rearrangement enables low-working-potential hard carbon toward sodium-ion batteries with enhanced energy density. Adv Mater 2024;36:2407369. https://doi.org/10.1002/adma.202407369.
[18] Zeng Y, Wang F, Cheng Y, Chen M, Hou J, Yang D, et al. Identifying the importance of functionalization evolution during pre-oxidation treatment in producing economical asphalt-derived hard carbon for Na-ion batteries. Energy Storage Mater 2024;73:103808. https://doi.org/10.1016/j.ensm.2024.103808.
[19] Zeng Y, Yang J, Yang H, Yang Y, Zhao J. Bridging microstructure and sodium-ion storage mechanism in hard carbon for sodium ion batteries. ACS Energy Lett 2024;9:1184–91. https://doi.org/10.1021/acsenergylett.3c02751.
[20] Chen X, Tian J, Li P, Fang Y, Fang Y, Liang X, et al. An overall understanding of sodium storage behaviors in hard carbons by an “adsorption-intercalation/filling” hybrid mechanism. Adv Energy Mater 2022;12:2200886. https://doi.org/10.1002/aenm.202200886.
[21] Ma M, Cai H, Xu C, Huang R, Wang S, Pan H, et al. Engineering solid electrolyte Interface at Nano-scale for high-performance hard carbon in sodium-ion batteries. Adv Funct Mater 2021;31:2100278. https://doi.org/10.1002/adfm.202100278.
[22] Cui K, Hou R, Zhou H, Guo S. Electrolyte engineering of hard carbon for sodium-ion batteries: from mechanism analysis to design strategies. Adv Funct Mater 2025:2419275. https://doi.org/10.1002/adfm.202419275.
[23] Zhang B, Chen G, Yang Y, Liu M, Li X, Liu H, et al. Heterovalent chromium-doped Na3Fe2(PO4)P2O7 cathode material with superior rate and stability performance for sodium-ion storage. ACS Sustain Chem Eng 2023;11:10083–94. https://doi.org/10.1021/acssuschemeng.3c02013.
[24] Wang X, Li H, Zhang W, Ge X, He L, Zhang L, et al. Unlocking fast and highly reversible sodium storage in Fe-based mixed polyanion cathodes for low-cost and high-performance sodium-ion batteries. J Mater Chem A 2023;11:6978–85. https://doi.org/10.1039/D3TA00014A.
[25] Feng X, Ren D, He X, Ouyang M. Mitigating thermal runaway of Lithium-ion batteries. Joule 2020;4:743–70. https://doi.org/10.1016/j.joule.2020.02.010.
[26] Wang Q, Ping P, Zhao X, Chu G, Sun J, Chen C. Thermal runaway caused fire and explosion of lithium ion battery. J Power Sources 2012;208:210–24. https://doi.org/10.1016/j.jpowsour.2012.02.038.
[27] Liu X, Ren D, Hsu H, Feng X, Xu G-L, Zhuang M, et al. Thermal runaway of Lithium-ion batteries without internal short circuit. Joule 2018;2:2047–64. https://doi.org/10.1016/j.joule.2018.06.015.
[28] Li Y, Lu Y, Chen L, Hu Y-S. Failure analysis with a focus on thermal aspect towards developing safer Na-ion batteries*. Chin Phys B 2020;29:048201. https://doi.org/10.1088/1674-1056/ab7906.
[29] Huang L, Xu G, Du X, Li J, Xie B, Liu H, et al. Uncovering LiH triggered thermal runaway mechanism of a high-energy LiNi0.5Co0.2Mn0.3O2/graphite pouch cell. Adv Sci 2021;8:2100676. https://doi.org/10.1002/advs.202100676.
[30] Jia H, Yang Z, Xu Y, Gao P, Zhong L, Kautz DJ, et al. Is nonflammability of electrolyte overrated in the overall safety performance of Lithium ion batteries? A sobering revelation from a completely nonflammable electrolyte. Adv Energy Mater 2023;13:2203144. https://doi.org/10.1002/aenm.202203144.
[31] Hou J, Feng X, Wang L, Liu X, Ohma A, Lu L, et al. Unlocking the self-supported thermal runaway of high-energy lithium-ion batteries. Energy Storage Mater 2021;39:395–402. https://doi.org/10.1016/j.ensm.2021.04.035.
[32] Wu Y, Liu Y, Feng X, Ma Z, Xu X, Ren D, et al. Smart solid-state interphases enable high-safety and high-energy practical Lithium batteries. Adv Sci 2025:2400600. https://doi.org/10.1002/advs.202400600.
[33] Li Y, Feng X, Ren D, Ouyang M, Lu L, Han X. Thermal runaway triggered by plated Lithium on the anode after fast charging. ACS Appl Mater Interfaces 2019. https://doi.org/10.1021/acsami.9b16589.
[34] Hou J, Lu L, Wang L, Ohma A, Ren D, Feng X, et al. Thermal runaway of Lithium-ion batteries employing LiN(SO2F)2-based concentrated electrolytes. Nat Commun 2020;11:5100. https://doi.org/10.1038/s41467-020-18868-w.
[35] Wang Y, Feng X, Peng Y, Zhang F, Ren D, Liu X, et al. Reductive gas manipulation at early self-heating stage enables controllable battery thermal failure. Joule 2022;6:2810–20. https://doi.org/10.1016/j.joule.2022.10.010.
[36] He Z, Li H, Ji W, Li W, Zhang Y, Li X, et al. Investigation on Li-plating prevention optimal charging protocol of nickel-rich/graphite-SiOx lithium ion battery. J Power Sources 2023;571:233044. https://doi.org/10.1016/j.jpowsour.2023.233044.
[37] Xue J, Zhang H, Chen J, Fang K, Chen Y, Zou Y, et al. Unlocking the Na-storage behavior in hard carbon anode by mass spectrometry. Nano Lett 2024;24:9839–45. https://doi.org/10.1021/acs.nanolett.4c01620.
[38] Chen X, Shen X, Li B, Peng H-J, Cheng X-B, Li B-Q, et al. Ion–solvent complexes promote gas evolution from electrolytes on a sodium metal anode. Angew Chem Int Ed 2018;57:734–7. https://doi.org/10.1002/anie.201711552.
[39] Cui H, Song Y, Ren D, Wang L, He X. Electrocapillary boosting electrode wetting for high-energy lithium-ion batteries. Joule 2024;8:29–44. https://doi.org/10.1016/j.joule.2023.11.012.
[40] Li C, Liang Z, Wang L, Cao D, Yin Y-C, Zuo D, et al. Superwettable electrolyte engineering for fast charging Li-ion batteries. ACS Energy Lett 2024;9:1295–304. https://doi.org/10.1021/acsenergylett.3c02572.
[41] Cui H, Ren D, Yi M, Hou S, Yang K, Liang H, et al. Operando monitoring of the open circuit voltage during electrolyte filling ensures high performance of lithium-ion batteries. Nano Energy 2022;104:107874. https://doi.org/10.1016/j.nanoen.2022.107874.